

# Methods and Results Sections of a Scientific Paper

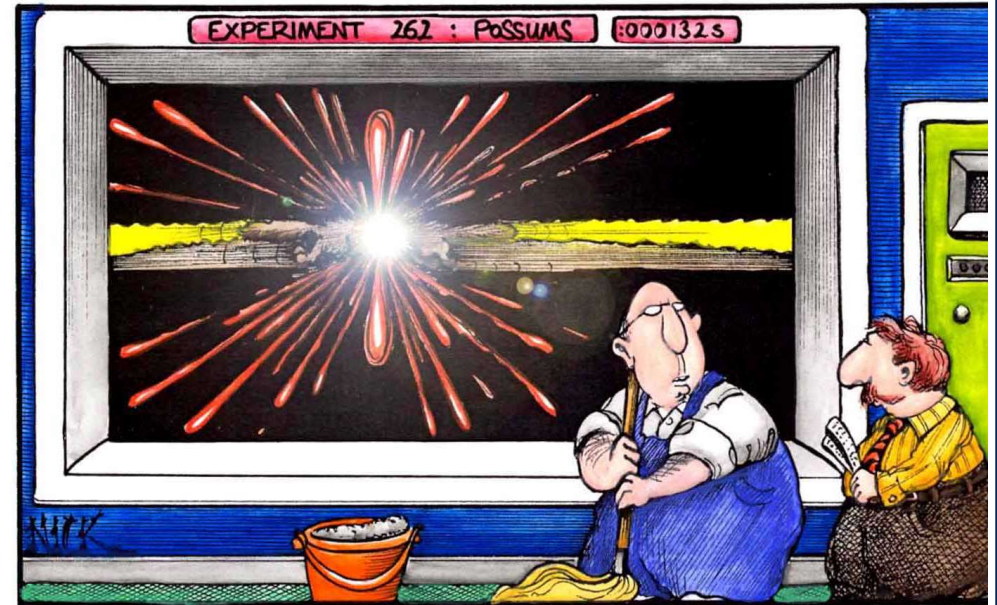
---



# Writing the Methods and Procedures Section

The purpose of this section is to describe the experimental or theoretical techniques and methods

STRANGE MATTER  
by nick d. kim  
strange-matter.com



**"Sure been a heap more work for ME around here since those Biologists got granted research time on the ol' Supercollider..."**

## Important Elements

Techniques used: Provide enough detail so that others can replicate and evaluate the experimental or theoretical arrangement used

Methods used: Describe general procedures used in obtaining your results, with sufficient detail for others to repeat the experiment or calculation and evaluate your methods

# Writing the Methods and Procedures Section

---

## Tips and Guidelines

Be precise in describing methods, e.g., give exact temperature values, measurement currents and voltages, etc.

You may not be able to use trade names (can be construed as advertising), unless this detail is critical to the method

Provide any references that might help the reader understand or repeat your methods

Don't introduce discussion, results, or conclusions in this section

Diagrams or figures of the experimental set-up or key parts of the apparatus are often useful—show scale and point out important features

Describe any methods used to extract or analyze the data

# Writing the Methods and Procedures Section

---

## Tips and Guidelines

It has been conventional to write this section in the third-person, active-voice, past tense to emphasize the measurement (rather than the person making the measurement) and to convey what was actually done:

“X-ray diffraction measurements were performed...”

However, it is becoming more common to write in the first person, past tense to emphasize what was actually done by the investigators:

“We performed X-ray diffraction measurements ...”

Write facts in the present tense:

“The 5-BM-D beamline at the Advanced Photon Source contains a dedicated extended x-ray absorption fine structure setup...”

## Measurement of the Damping of the Nuclear Shell Effect in the Doubly Magic $^{208}\text{Pb}$ Region

P. C. Rout,<sup>1,2,\*</sup> D. R. Chakrabarty,<sup>1,2</sup> V. M. Datar,<sup>1,2</sup> Suresh Kumar,<sup>1,2</sup> E. T. Mirgule,<sup>1</sup> A. Mitra,<sup>1</sup>  
V. Nanal,<sup>3</sup> S. P. Behera,<sup>1,2</sup> and V. Singh<sup>2,4</sup>

Third person,  
past tense



Notice the detail in  
the descriptions!

The experiment was performed at the Mumbai Pelletron Linac Facility using a 30 MeV pulsed  $^7\text{Li}$  beam of width  $\sim 1.5$  ns (FWHM) and period  $\sim 107$  ns. Self-supporting foils of  $4.7 \text{ mg/cm}^2$   $^{205}\text{Tl}$  (enriched to  $>99\%$ ) and  $3.7 \text{ mg/cm}^2$   $^{181}\text{Ta}$  ( $\sim 100\%$  natural abundance) were used as targets. Alpha particles were detected at backward angles ( $\sim 126^\circ$ – $150^\circ$ ) in 8 CsI(Tl) detectors of dimensions  $2.5 \text{ cm} \times 2.5 \text{ cm} \times 1 \text{ cm}$  (thick) coupled to Si(*P-I-N*) photodiodes and placed at a distance of  $\sim 5$  cm from the target. The detectors were covered with an aluminized mylar foil of thickness  $\sim 1 \mu\text{m}$ . Particle identification was done using the standard pulse shape discrimination method by measuring the zero crossover timing (ZCT) of the amplified bipolar pulse.

Neutrons were detected using an array of 15 plastic detectors each of dimension  $6 \text{ cm} \times 6 \text{ cm} \times 100 \text{ cm}$  viewed by two photomultipliers, one at each end [15]. The array was placed at a mean angle of  $90^\circ$  to the beam direction and at a distance of 1 m from the target. The neutron energy was measured using the time of flight (TOF) technique. The data were collected in an event by event mode using a CAMAC based data acquisition system. The parameters recorded were (a) left and right timing of each plastic detector with respect to rf from the beam pulsing system using time to digital converters, (b) integrated charge of anode pulses (which is related to the electron equivalent energy,  $E_{ee}$ , deposited in the plastic detector) from the left and right photomultipliers using charge to digital converters, (c) timing of CsI(Tl) detectors with respect to the pulsed beam, (d) energy deposited in the CsI(Tl) detectors ( $E_{\text{CsI}}$ ), and (e) ZCT of the CsI detectors.





## Pseudospin-Resolved Transport Spectroscopy of the Kondo Effect in a Double Quantum Dot

S. Amasha,<sup>1</sup> A. J. Keller,<sup>1</sup> I. G. Rau,<sup>2,\*</sup> A. Carmi,<sup>3</sup> J. A. Katine,<sup>4</sup> Hadas Shtrikman,<sup>3</sup> Y. Oreg,<sup>3</sup> and  
D. Goldhaber-Gordon<sup>1,3,†</sup>

In this Letter, we report pseudospin-resolved transport spectroscopy of the Kondo effect based on an orbital degeneracy in a DQD. We first demonstrate spectroscopy of the DQD analogous to standard transport spectroscopy in a single dot, and we use this to observe the zero-bias peak that is the hallmark of Kondo physics. In standard spectroscopy of spin Kondo, a magnetic field splits the Kondo peak so that the conductance at zero bias is suppressed and the Kondo peaks occur at positive and negative bias. In contrast, pseudospin-resolved spectroscopy of the orbital Kondo effect in a pseudomagnetic field shows a peak at only one sign of the bias, corresponding to the pseudospin state we are observing. Finally, we demonstrate that a single, consistent Kondo temperature can be defined for the entire DQD system.

We measure a laterally gated DQD fabricated from an epitaxially grown AlGaAs/GaAs heterostructure hosting a two-dimensional electron gas with a density of  $2 \times 10^{11} \text{ cm}^{-2}$  and a mobility of  $2 \times 10^6 \text{ cm}^2/\text{V s}$ . We apply negative voltages to metallic surface gates (inset of Fig. 1) to form two capacitively coupled quantum dots with negligible interdot tunneling [26]. The gates W1L and W1U control the tunneling rates between dot 1 and its source and drain leads  $\Gamma_{S1}/\hbar$  and  $\Gamma_{D1}/\hbar$ , respectively. We define  $\Gamma_1 = \Gamma_{S1} + \Gamma_{D1}$ , and  $\Gamma_2$  analogously for dot 2. The conductances of the dots are measured using separate circuits. All the

First person,  
present tense is  
becoming more  
common!





## Observation of Spin Correlation in $t\bar{t}$ Events from $pp$ Collisions at $\sqrt{s} = 7$ TeV Using the ATLAS Detector

beyond the SM predict different spin correlations while keeping the  $t\bar{t}$  production cross section within experimental and theoretical bounds [14–18]. For example, the spin correlation measured in this Letter may differ from the SM if the  $t\bar{t}$  pairs were produced via the exchange of a virtual heavy scalar Higgs boson [19] or if the top quark decayed into a scalar charged Higgs boson and a  $b$  quark ( $t \rightarrow H^+ b$ ) [20].

At the LHC  $t\bar{t}$  production occurs mostly through the  $gg \rightarrow t\bar{t}$  channel. At low  $t\bar{t}$  invariant mass it is dominated by the fusion of like-helicity gluon pairs which produce top quarks in the left-left or right-right helicity configurations [13]. When these decay via  $t\bar{t} \rightarrow W^+ W^- b\bar{b} \rightarrow l^+ \nu l^- \bar{\nu} b\bar{b}$  they produce charged leptons which possess correlations in azimuthal angle,  $\Delta\phi$  [21], in the laboratory frame [13]. In contrast, at the Tevatron production via  $q\bar{q}$  annihilation dominates. The different production mechanisms and center-of-mass energies make a measurement of the spin correlation at both colliders complementary [22]. Both the CDF and D0 Collaborations have performed measurements of the spin correlation [23–25], with a recent analysis by the D0 Collaboration reporting evidence for the presence of spin correlation in  $t\bar{t}$  events with a significance of 3.1 standard deviations [26].

First person,  
present tense  
(conveys a “fact” that  
is “always true”)

First person,  
present perfect  
tense  
(conveys something  
that was done but  
continues)


## Nuclear Quantum Effects and Nonlocal Exchange-Correlation Functionals Applied to Liquid Hydrogen at High Pressure

Miguel A. Morales,<sup>1,\*</sup> Jeffrey M. McMahon,<sup>2</sup> Carlo Pierleoni,<sup>3</sup> and David M. Ceperley<sup>2</sup>

In this Letter, we present results from FP simulations based on PIMD to treat NQEs, but using nonlocal DFs in DFT. These calculations remove one of the most significant approximations made in a number of previous simulations (classical protons), while at the same time improve over another equally important and heretofore less-considered approximation (local or semilocal DFs). Such calculations allow us to study molecular dissociation in hydrogen with previously unattainable accuracy.

Simulations were performed via DFT, and we focused on two nonlocal DFs. We first chose to use the Heyd–Scuseria–Ernzerhof (HSE) DF [32], which is known to have a very small self-interaction error [33]. We also performed simulations with the second version of the van der Waals density functional (vdW-DF2) [34–37], which provides a reasonable description to exchange (for a semi-local functional), but moreover provides an improved description of nonlocal correlation (dispersion interactions) in DFT. Simulations with the former were performed

First person, past tense  
(what was done)



Present tense (a fact)





## Writing the Results Section

---

The purpose of this section is to objectively present your findings. Generally, it's a good idea to make this section a completely objective report of your results, and to save any interpretation and comparison with working hypotheses for a separate Discussion Section



### Important Elements

Summary of results: Describe the key results obtained, with accompanying figures and graphs of raw results

Analyzed data: Present any “converted” data obtained from an analysis of the raw data. Make sure to describe what conversion procedure was used

Relevant details: Highlight for the reader any noteworthy observations

# Writing the Results Section

---

## Tips and Guidelines

Try not to interpret, or draw conclusions from, your results in this section: Strive for a clear separation between your (presumably correct) results/calculations and your interpretations (discussion) of those results, which not everyone may agree with.

Describe things that were done in the past tense, but refer to “facts” in the present tense

Present your results in some logical order designed to support your key conclusions (chronological order is generally not the best way). **Usually it's best to start with figures and tell a story about your research.**

Present your results as clearly and concisely as possible

# Example Methods Section

PRL 110, 067202 (2013)

PHYSICAL REVIEW

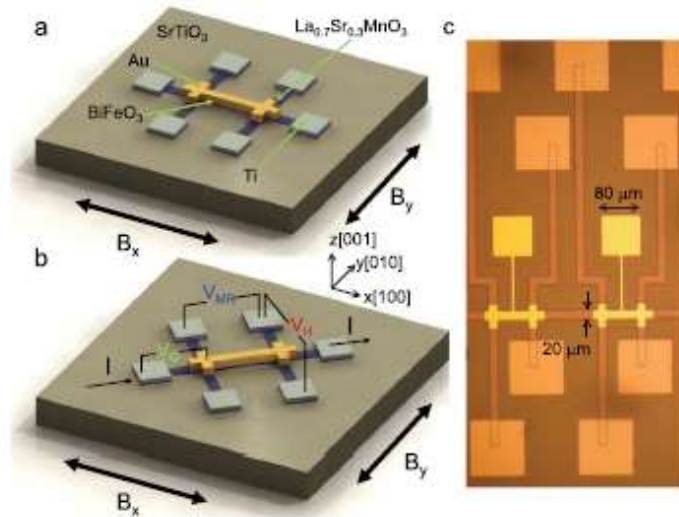


FIG. 1 (color online). (a), (b) Two devices with a gated hall bar geometry. In (a) current goes in the [100] direction, while in (b) the current goes along [110]. Voltage pulses ( $V_G$ ) are applied to the Au top gate electrode to ferroelectrically polarize BFO and the four point magnetoresistivity of LSMO is measured under applied fields in both the  $x$  and  $y$  directions. (c) An optical photograph of the device.

To investigate the magnetic properties of the LSMO channel, we measured its electrical resistance as a function of applied in-plane magnetic field in both the [100] ( $B_x$ ) and [010] ( $B_y$ ) directions, separately, as depicted in Figs. 1(a) and 1(b). Each magnetotransport measurement is performed at a static temperature, and at no point in the experiment was the device cooled in any electric or magnetic field. Typical measurements for both BFO FE polarizations are shown in Fig. S1 of the Supplemental Material [11]. The data exhibit magnetic hysteresis and have coercive and saturation features analogous to that of an  $M-H$  hysteresis loop. We interpret the peaks in resistance as the coercive fields where there is zero net magnetization and that the tail is where magnetization becomes saturated. By determining these peak positions we determine the magnetic coercivity (distance between the peaks) and exchange bias (shift in the peaks off the origin) as shown in Fig. S1 [11]. Results using this technique are in excellent agreement with SQUID magnetometer  $M-H$  measurements on unpatterned films and are further detailed in our previous work on such devices [9].

To examine the effect of BFO polarization on exchange bias, a  $\pm 24$  V voltage pulse was applied between the gate and the LSMO channel to polarize the BFO in the [001] direction. Measurements show that BFO polarization out of plane is fully saturated; however, complex domain structures may still form in plane since there are still four degenerate in-plane polarization states [9]. These structures are difficult to observe in our device due to the Au top electrode, but we can draw parallels from piezoresponse-force microscopy images for unpatterned BFO-LSMO heterostructures from previous work [9]. Magnetoresistance is measured and exchange bias is then

The authors use first person, present tense;  
Note that they just tell a story about their figure



## Example Results Section

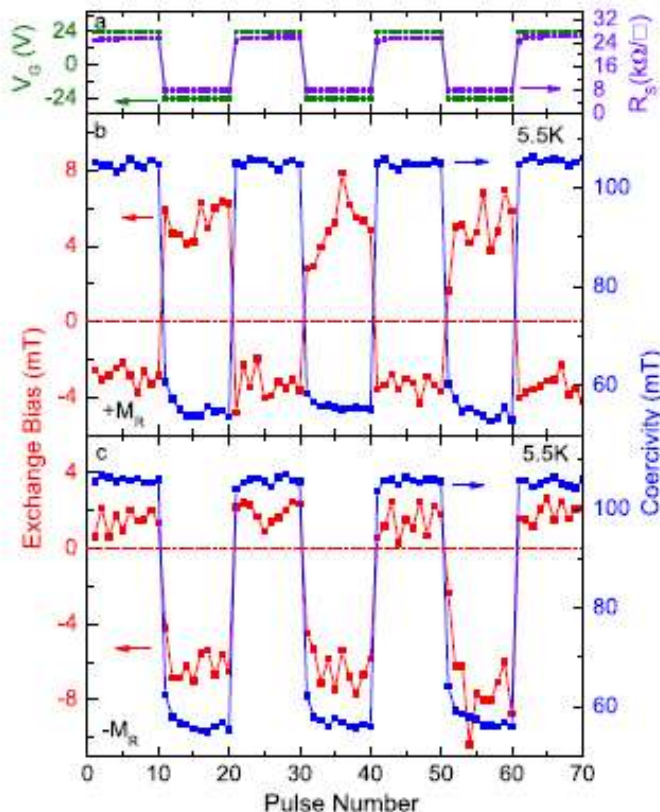


FIG. 2 (color online). (a) Gate pulse sequence applied before carrying out magnetoresistance measurements (green, left arrow) and the corresponding sheet resistance of the LSMO (purple, right arrow). (b), (c) Measurements of exchange bias and coercivity taken at 5.5 K after gate pulse shown in (a). Panels (b) and (c) represent the data when voltage pulses are applied in positive and negative remanent magnetization, respectively. Current was applied along the [110] direction with applied magnetic field in the  $B_x$  [100] direction.

PRL 110, 067202 (2013)

PHYSICAL REVIEW

on three separate epitaxially grown heterostructures. Figures 2(b) and 2(c) show bipolar modulation with respect to gate pulse at 5.5 K in both remanent magnetization states for a device patterned along the [110] [Fig. 1(b)] direction with magnetic field applied in [100] ( $B_x$ ). Depending on the remanent magnetization state of LSMO upon application of gate pulses, opposite FE polarizations lead to opposite directions of exchange bias. The modulation behavior is mirrored through the zero exchange bias axis between different remanent magnetization states. The temperature of the sample was held at 5.5 K throughout the measurement. The sole determining factors for the polarity of exchange bias in these bipolar devices are (a) the polarization state of the BFO film and (b) the  $M_R$  of LSMO. To offer a comparison of the bipolar modulation behavior to unipolar modulation, a plot is presented in the supplemental figure Fig. S2 [11].

Notice how the authors are just telling a story about their figure and stating the facts of their data



## Example Results Section

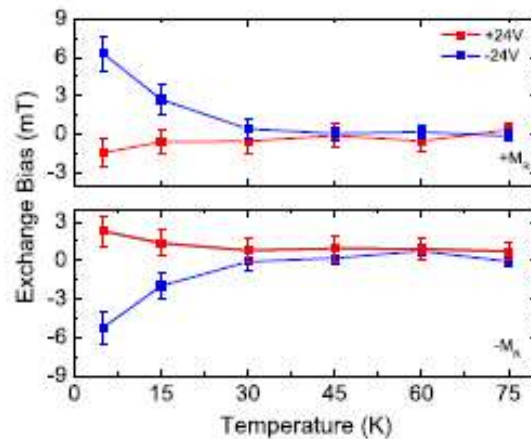


FIG. 3 (color online). Exchange bias as a function of temperature for both remanent magnetization states of LSMO for a device oriented in the [110] direction with magnetic field applied in the  $B_x$  [100] direction.

Temperature dependent measurements of exchange bias were taken. Following the same protocol outlined above, exchange bias in both remanent magnetizations was measured at different temperatures (Fig. 3). We observe that there is bipolar modulation in both remanent magnetization states of the LSMO with a decay towards zero exchange bias in both states as temperature is increased. The magnitude of exchange bias is always smaller in the positive BFO polarization state, which corresponds to the high electrical resistivity or magnetic coercivity state.

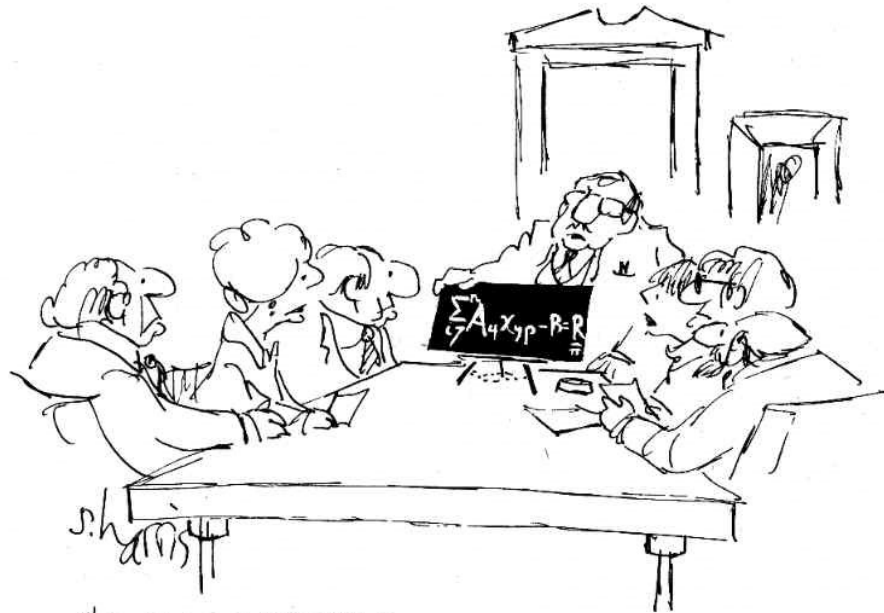
The authors characterize their results, but they do not interpret what the results mean in this section

Again, they're telling a story about their figure...this is why it helps to generate your figures first!

# The Discussion Section

---

The goal of this section is to provide an interpretation of your results, support for your conclusions, and a comparison of your results to relevant hypotheses



"LADIES AND GENTLEMEN, OUR RESEARCH DEPARTMENT HAS COME UP WITH THIS. WHAT DO WE WISH TO DO WITH IT?"

## Important Elements

Detailed Analysis: Analyze your results with an appropriate level of detail. Compare your results with previous results.

Hypothesis testing: If your results agree with or differ from particular models, provide an explanation of the relevant hypotheses, and explain in detail why you believe your results agree or disagree with these models

# The Discussion Section

VIEW LETTERS

week ending  
8 FEBRUARY 2013

Modulation disappears around 30 K, well below the blocking temperature of this system which was previously determined to be around 100–120 K.

We can now speculate on the mechanism behind the electric field control of exchange bias in this system. The most recent exchange bias models are based on the existence of an interface state between the AFM and FM that is markedly different than either the FM or the AFM individually [12]. Such an interface state will produce two different types of spins that contribute unequally to the exchange bias system [13–16]. Some interface spins will become pinned in a single direction by the AFM, unaffected by magnetic field. The interaction between these pinned spins and the FM causes an effective “bias field” that the underlying FM layer must overcome before magnetization can be switched, resulting in exchange bias. Other interface spins will rotate with the FM layer when the magnetic field is swept, because they are coupled more tightly to the FM than the AFM. This results in a spin drag effect that increases the coercivity of the FM material. Several groups have observed these types of magnetic interface interactions [5,6]. Previous work showed an emergent interfacial magnetic state, correlated with exchange bias, in BFO-LSMO heterostructures resulting from the enhanced canting of the AFM spins at an otherwise magnetically compensated interface [17]. Furthermore, in this system the coupling between  $\text{Fe}^{3+}$  in the magnetic interface layer and the  $\text{Mn}^{3+/4+}$  was antiferromagnetic. Many exchange bias systems exhibit this type of AFM interfacial coupling, but no differences in exchange bias occur until extremely high magnetic fields are applied to overcome the interfacial coupling and align all spins to the external magnetic field. Since we do not use such high fields, the exchange bias model described above does not change. Some spins will be pinned, and some will rotate with the FM; since the coupling to the interface layer is antiferromagnetic, the interface spins will evolve in the opposite fashion as compared to the ferromagnetically coupled case [18].

← Now you can speculate!



# The Discussion Section

VIEW LETTERS

week ending  
8 FEBRUARY 2013

Modulation disappears around 30 K, well below the blocking temperature of this system which was previously determined to be around 100–120 K.

We can now speculate on the mechanism behind the electric field control of exchange bias in this system. The most recent exchange bias models are based on the existence of an interface state between the AFM and FM that is markedly different than either the FM or the AFM individually [12]. Such an interface state will produce two different types of spins that contribute unequally to the exchange bias system [13–16]. Some interface spins will become pinned in a single direction by the AFM, unaffected by magnetic field. The interaction between these pinned spins and the FM causes an effective “bias field” that the underlying FM layer must overcome before magnetization can be switched, resulting in exchange bias. Other interface spins will rotate with the FM layer when the magnetic field is swept, because they are coupled more tightly to the FM than the AFM. This results in a spin drag effect that increases the coercivity of the FM material.

Several groups have observed these types of magnetic interface interactions [5,6]. Previous work showed an emergent interfacial magnetic state, correlated with exchange bias, in BFO-LSMO heterostructures resulting from the enhanced canting of the AFM spins at an otherwise magnetically compensated interface [17]. Furthermore, in this system the coupling between  $\text{Fe}^{3+}$  in the magnetic interface layer and the  $\text{Mn}^{3+/4+}$  was antiferromagnetic. Many exchange bias systems exhibit this type of AFM interfacial coupling, but no differences in exchange bias occur until extremely high magnetic fields are applied to overcome the interfacial coupling and align all spins to the external magnetic field. Since we do not use such high fields, the exchange bias model described above does not change. Some spins will be pinned, and some will rotate with the FM; since the coupling to the interface layer is antiferromagnetic, the interface spins will evolve in the opposite fashion as compared to the ferromagnetically coupled case [18].

← Comparison with models



# The Discussion Section

VIEW LETTERS

week ending  
8 FEBRUARY 2013

Modulation disappears around 30 K, well below the blocking temperature of this system which was previously determined to be around 100–120 K.

We can now speculate on the mechanism behind the electric field control of exchange bias in this system. The most recent exchange bias models are based on the existence of an interface state between the AFM and FM that is markedly different than either the FM or the AFM individually [12]. Such an interface state will produce two different types of spins that contribute unequally to the exchange bias system [13–16]. Some interface spins will become pinned in a single direction by the AFM, unaffected by magnetic field. The interaction between these pinned spins and the FM causes an effective “bias field” that the underlying FM layer must overcome before magnetization can be switched, resulting in exchange bias. Other interface spins will rotate with the FM layer when the magnetic field is swept, because they are coupled more tightly to the FM than the AFM. This results in a spin drag effect that increases the coercivity of the FM material.

Several groups have observed these types of magnetic interface interactions [5,6]. Previous work showed an emergent interfacial magnetic state, correlated with exchange bias, in BFO-LSMO heterostructures resulting from the enhanced canting of the AFM spins at an otherwise magnetically compensated interface [17]. Furthermore, in this system the coupling between  $\text{Fe}^{3+}$  in the magnetic interface layer and the  $\text{Mn}^{3+/4+}$  was antiferromagnetic. Many exchange bias systems exhibit this type of AFM interfacial coupling, but no differences in exchange bias occur until extremely high magnetic fields are applied to overcome the interfacial coupling and align all spins to the external magnetic field. Since we do not use such high fields, the exchange bias model described above does not change. Some spins will be pinned, and some will rotate with the FM; since the coupling to the interface layer is antiferromagnetic, the interface spins will evolve in the opposite fashion as compared to the ferromagnetically coupled case [18].

← Comparison with previous data

# The Discussion Section

---

romagnetic. Many exchange bias systems exhibit this type of AFM interfacial coupling, but no differences in exchange bias occur until extremely high magnetic fields are applied to overcome the interfacial coupling and align all spins to the external magnetic field. Since we do not use such high fields, the exchange bias model described above does not change. Some spins will be pinned, and some will rotate with the FM; since the coupling to the interface layer is antiferromagnetic, the interface spins will evolve in the opposite fashion as compared to the ferromagnetically coupled case [18].

Based on these models we present an explanation for the following effects: bipolar exchange bias modulation, the remanent magnetization dependence of that modulation, and coercivity modulation. The progression of the magnetic state in our device as magnetic field is swept and after a gate pulse reverses BFO polarization is shown in Fig. 4. Figure 4(a) shows the progression in terms of a magnetic hysteresis loop and Fig. 4(b) shows it from an interfacial spin state perspective. Because of the ferroelectric nature of BFO, when ferroelectric polarization is switched, the Fe and Bi ions will move relative to the oxygen octahedra [19]. Since the LSMO channel does not exhibit the same effect, the Fe ion at the interface in BFO exists in two different states depending on FE polarization, one closer to the LSMO channel and one farther away. The AFM anisotropy is much greater than the FM anisotropy [20,21];

← Interpretation of results

# Another *Physical Review Letters* Example: Results Section

PRL 110, 065702 (2013)

PHYSICAL REVIEW LETTERS

week ending  
8 FEBRUARY 2013

## Nuclear Quantum Effects and Nonlocal Exchange-Correlation Functionals Applied to Liquid Hydrogen at High Pressure

Miguel A. Morales,<sup>1,\*</sup> Jeffrey M. McMahon,<sup>2</sup> Carlo Pierleoni,<sup>3</sup> and David M. Ceperley<sup>2</sup>

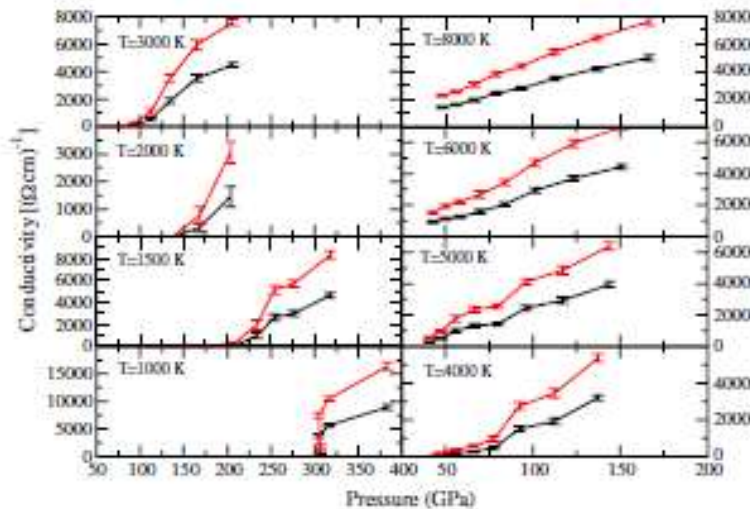


FIG. 4 (color online). Electronic conductivity as a function of pressure, along various isotherms. Results calculated with both HSE (black, lower line) and PBE (red, higher line) DFs are shown for comparison.

Figure 4 shows the electronic conductivity as a function of pressure along various isotherms, comparing both PBE and HSE DFs. Note that in both cases, proton configuration were generated with vdW-DF2. Notice also that while the conductivity values differ between HSE and PBE DFs, they nonetheless agree on the *existence* of a jump at  $T = 1000$  K.

Returning to Fig. 1, a schematic phase diagram of hydrogen in the regime of molecular dissociation and below


Presentation of results;  
Note that you can characterize your results, just don't interpret them here.



# The Discussion Section

---

Comparison  
with previous  
results



PRL 110, 065702 (2013)

PHYSICAL REVIEW LETTERS

$T = 6000$  K can be seen. The previously reported LLPT, obtained with classical protons and either from FPMD + PBE or coupled electron-ion Monte Carlo (CEIMC) [21] calculations are shown [49]. Both vdW-DF2 (present work) and CEIMC calculations show a considerable increase in the transition pressures with respect to PBE DFs, with those from vdW-DF2 being considerably higher. Above the critical point, state points of an electronic conductivity of  $\sigma = 2000 (\Omega \text{ cm})^{-1}$ , separating the insulating from metallic liquid [50], are also reported using either vdW-DF2 or PBE. Loubeyre *et al.* [47] reported that the metal-to-insulating threshold was located at conditions of 10% reflectivity, since according to the Drude model, this corresponds to an ionization of 1%. The present criterion for metallic behavior is different though. For example, from our reflectivity data, a minimum metallic conductivity of  $\sigma = 2000 (\Omega \text{ cm})^{-1}$  corresponds to a reflectivity of  $\sim 0.35\text{--}0.40$  which is closer to 70% of its saturation value ( $\sim 0.6$ ). This explains why our threshold line is in apparent disagreement with the experimental points reported in Ref. [47]. In fact, at conditions of 10% reflectivity, close to the precompressed-state Hugoniot curve, we observe conductivities on the order of  $\sigma = 100\text{--}500 (\Omega \text{ cm})^{-1}$ . Figure 1 also shows the result from the reverberation shock compression of S. Weir *et al.* [50]. While the temperature was not measured therein experimentally, but rather estimated using a model EOS, and the error bars were rather large, it is nonetheless clear that the presented results of the location of the LLPT and the dissociation regime at higher temperatures agree rather well.

While almost all FP simulation methods agree qualitatively on the existence of a first-order LLPT in high-



## The Discussion Section

---

large, it is nonetheless clear that the presented results of the location of the LLPT and the dissociation regime at higher temperatures agree rather well.

While almost all FP simulation methods agree qualitatively on the existence of a first-order LLPT in high-pressure hydrogen [21,23], its precise location depends on the approximations employed. The results reported above clearly show that NQEs and nonlocal DFs in DFT play an important role in the description of molecular dissociation and metallization. The two DFs considered (HSE and vdW-DF2) were originally developed with the goal of addressing significant limitations of local and semi-local DFs in DFT. HSE, on the one hand, was developed to reduce self-interaction errors in PBE in its applications to solids [32]. Such errors lead to a strong tendency to favor delocalized electronic states, which in turn lead to an underestimation of band gaps by as much as 1–2 eV (in hydrogen) [24]. This leads to a serious underestimation of the metallization pressures in both liquid and solid phases, and a tendency to favor metallic states (e.g., solid structures). vdW-DF and its improved version vdW-DF2 (employed in this work), on the other hand, were developed to account for nonlocal electron correlations, such as dispersion interactions in DFT. The presented results indicate that, at least close to dissociation, both HSE and vdW-DF2 DFs produce very similar structures in liquid hydrogen. Since the physical effects addressed by both DFs are not directly related to each other, and that both effects are expected to be relevant in the molecular phase, it is important to recognize that the LLPT pressures might still

Interpretation of  
results



change if a DF which combines both hybrid exchange and nonlocal correlation were to be employed.

The goal of this Letter was not to predict which functional (HSE or vdW-DF2, etc.) is more accurate, since answering that question requires the use of more accurate methods [51]. We can however mention several possibilities that explain the observed behavior, the reasonable agreement between either nonlocal DF as well as their large disagreements with PBE DFs. Both DFs predict shorter molecular bonds compared to PBE; in the limit of low density, the bond length predicted by vdW-DF2 agrees very well with measured values while that of PBE DFs is overestimated by  $\sim 3\%$  [52]. This is obviously an important factor on dissociation. Second, the exchange portion of the vdW-DF2 functional was constructed to reproduce exact-exchange results [37], which may explain its similarity to HSE. Finally, both dispersion interactions and a reduced self-interaction will lead to a more stable molecular state. An even more promising alternative to DFT is the use of quantum Monte Carlo first-principles methods, for example CEIMC [21], using accurate trial wave functions, such as those constructed from HSE orbitals. We must also recognize that, while the use of the vdW-DF2 DF made large improvements in the description of molecular dissociation in hydrogen near the LLPT, standard semilocal DFs like PBE have been shown to be successful in describing other materials when combined with the HSE DF for the calculation of optical properties [53].

Discussion of  
different  
interpretations



# Informal homework assignment

---

Using your journal club/referee report paper selection:

Evaluate the Methods and Procedures section of your paper to study and critique how the authors discuss their methods. Do they provide sufficient detail? Is this section clear? Do you like the style they've adopted?

Then evaluate the Results and Discussion sections of your paper to study and critique how the authors discuss their methods. Is there a clear separation between the results presented and the discussion/analysis of these results? Do the authors tell a good story with their figures and discussion?